Eur. Phys. J. Plus (2020) 135:600
https://doi.org/10.1140/epjp/s13360-020-00606-2

THE EUROPEAN PHYSICAL JOURNAL PLUS

Regular Article

Internal heat generation on bioconvection of an MHD nanofluid flow due to gyrotactic microorganisms

Gangadhar Kotha[1,a], **Venkata Ramana Kolipaula**[2,b], **Munagala Venkata Subba Rao**[3,c], **Surekha Penki**[1,d], **Ali J. Chamkha**[4,5,e]

[1] Department of Mathematics, Acharya Nagarjuna University Campus, Ongole, Andhra Pradesh 523001, India
[2] Department of Mathematics, Vignan's Lara Institute of Technology and Science, Vadlamudi, Guntur, Andhra Pradesh 522213, India
[3] Division of Mathematics, Department of Sciences and Humanities, Vignan's Foundation for Science, Technology and Research, Vadlamudi, Andhra Pradesh 522 213, India
[4] Institute of Research and Development, Duy Tan University, Da Nang 550000, Vietnam
[5] Institute of Theoretical and Applied Research (ITAR), Duy Tan University, Hanoi 100000, Vietnam

Received: 1 June 2020 / Accepted: 13 July 2020

Abstract The principal aim of this paper is to analyse the two-dimensional magnetohydrodynamic flow and heat and mass transfer phenomena of water-based nanofluid containing gyrotactic microorganisms over a vertical plate by means of heat generation or absorption. Set of nonlinear ordinary differential equations are derived from the governing partial differential equations of the two-dimensional flow of MHD nanofluid and nanoparticles by utilizing appropriate similarity transformations. The numerical results are obtained with the proposed novel spectral relaxation method. The results revealed that in the heat and mass transfer, the motile microorganism flux rates as well as the velocity profiles are decreased throughout the fluid medium with the impact of magnetic field strength. Moreover, the drag stress rate and motile microorganism profiles are increased with the enhancement of magnetic field. Even though the problem of nanofluid has been broadly investigated, limited discoveries can be found through a gyrotactic microorganisms. Indeed, this paper managed to obtain the numerical analysis is performed. Furthermore, the authors also considered the MHD phenomena, heat generation or absorption effects. Very few studies in the fluid with gyrotactic microorganisms embedded in this parameter in their problems.

1 Introduction

At present, the industry and many research laboratories need highly efficient heat transfer scenarios. An acknowledged truth is that fluids, for example oils, water and kerosene, are very less in heat transport features and it is the main hurdle to the performance of industrial

[a] e-mail: kgangadharmaths@gmail.com
[b] e-mail: ramana.may@gmail.com
[c] e-mail: mail2mvsr@gmail.com
[d] e-mail: Surekha.penki@gmail.com
[e] e-mail: alichamkha@duytan.edu.vn (corresponding author)

Published online: 25 July 2020

items. In this process many new techniques are developed to enhance heat exchange rate in these fluids. As a result, nanofluids are introduced to improve the thermal efficiency in the base fluids because there are many applications in industry as well as engineering fields with heat transfer problems. In fact, nanofluids are emerging fluids that consist of nanosized solid particles that are distributed in convectional heat transfer fluids. These are formed by suspending either nonmetallic, metallic nanoparticles (below 100 mm diameter) in convectional fluids of heat transfer like toluene mineral oils or water [5]. Furthermore, the significant property of these fluids is better in thermal conductivity when compared to the base fluids, which can be accomplished even at a low nanoparticles' volume fraction. Nanofluids convective heat transport study is exhibited by Buongiorno [4]. Modelling of heat transfer past a vertical plate by considering distinct nanofluids is acknowledged by Rana and Bhargava [34], and on a linearly stretched surface, Khan and Pop [22] analysed the nanofluid flow and heat transfer analysis. Some critical reviewers [1, 9, 11–14, 16, 18, 28, 35, 36, 38, 39, 41, 44, 46] have been worked out on the transport phenomena of different nanofluids.

Further, microorganisms in viscous fluids flow become a research area to the scientists by the applications like scientific, agriculture and industrial applications. Microorganisms play a vital role in a lot of situations like toxin removal, food digestion and antibiotics. Mixing of fluids provided by suspension of microorganisms results in an augmented mass transfer. Knowing the properties of heat transfer is essential due to model of novel microfluidic devices. Fluid flow contains magnetic field is required in some applications.

In these fluids, an analysis of bioconvection plays a vital role and the term bioconvection is represented as the behaviour of microorganisms in the directions of downward and upward. Parameters are represented by viscous drag and gravity effects of the directional movement of microorganisms. Bioconvection Rayleigh number plays an important role in the examination of transmission of heat and mass of fluids possessing suspension of attenuate microorganisms. Steadiness of two-dimensional gyrotactic plumes was investigated by [17].

Later, [24] introduced nanofluid bioconvection model. Nanofluids consist of gyrotactic microorganisms and repeat the consequential large-scale motion of fluid affected by self-propelled motile microorganisms enhancing mixing and avoiding agglomeration of nanoparticle that was focused by Kuznetsov [25]. Ratio of buoyancy and viscous forces gives bioconvection Rayleigh number and is affected by density of microorganism's fluctuations and temperature difference, and it denotes the strength of convection [40]. An elaborated research [2, 7, 8, 10, 15, 20, 21, 26, 27, 29, 33, 42] is on bioconvection with suspensions of oxytactic bacteria and is formed to the onset of bioconvection in a deferment of gyrotactic/oxytactic microorganisms in various situations. They exhibited stability analysis and resoluted the impact of solid particles of small size in a dilute suspension consisting of gyrotactic microorganisms, and the impact of bioconvection in small solid particles was identified by the topic of effective diffusivity.

From all the above-mentioned examinations, the present analysis is motivated to reveal the flow and heat transfer characteristics of MHD nanofluid flow with motile gyrotactic microorganisms past a vertical plate in the presence of heat generation/absorption and motile gyrotactic microorganisms. As per the knowledge of author's concern, no study regarding the problem of heat and mass past a vertical plate in the occurrence of magnetic field, internal heat generation/absorption and motile gyrotactic microorganisms is investigated theoretically. The governing equations of the present flow problem are changed into the nonlinear system by utilizing the appropriate similarity transformations and solved numerically by utilizing the spectral relaxation method. All the numerical values of various parameters encountered in this study are presented as graphs and tables by assigning different estimations. To ensure

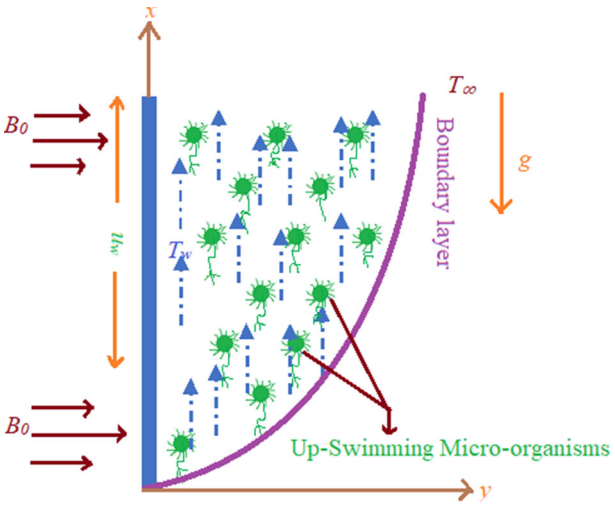

Fig. 1 Flow configuration and coordinate system

the precision and validness of the current thought outcomes of this study are compared under specified conditions. A decent concurrence is observed between the proposed study results, and previously recorded outcomes are available in the literature. The problem is original.

2 Mathematical formulation

Let us assume a water-based nanofluid, comprising electrically conduction and chemically reacting nanosolid particles and gyrotactic microorganisms by the assumption of water-based nanofluid as shown in Fig. 1. An assumption is taken that the hanging nanoparticles can be reserved steadily and do not aggregate in the fluid. One more assumption is considered that the nanoparticle does not produce any impact on velocity of microorganisms. Nanoparticles concentration less than 1% is defensible inference. So, bioconvection stability is considered as the suspension of solid nanoparticles and is diluted in the liquid medium. By the above considerations, the subsequent equations that are conversion of thermal energy, total mass, nanoparticles volume fraction, momentum and microorganisms can be found by the model of nanofluid given by Kuznetsov and Nield [26] and model as follows:

$$\nabla \cdot \bar{a} = 0, \tag{1}$$

$$\rho_f (\bar{a} \cdot \nabla) \cdot \bar{a} = -\nabla p + \mu \nabla^2 \bar{a} + \{C\rho_p + [\rho_f(1 - \beta (T - T_\infty))](1 - C) + \upsilon \Delta\rho N\} g_0 + \sigma (J \times B), \tag{2}$$

$$\bar{a} \cdot \nabla T = \alpha \nabla^2 T + \tau \left[D_B \nabla T \cdot \nabla C + \left(\frac{D_T}{T_\infty} \right) \nabla T \cdot \nabla T \right] + q''', \tag{3}$$

$$(\bar{a} \cdot \nabla) C = D_B \nabla^2 C + \left(\frac{D_T}{T_\infty} \right) \nabla^2 T, \tag{4}$$

$$\nabla . j = 0, \tag{5}$$

In the above equations $\bar{a} = (a_1, a_2, a_2)$ denotes flow velocity of nanofluid, T denotes temperature, p denotes pressure, C denotes concentration of nanoparticle, N denotes microorganisms concentration, ρ_{f} denotes density of nanofluid, j denotes microorganisms flux by diffusion, self-propelled swimming and fluid convection, ρ_{p} denotes density of the nanoparticles, μ denotes viscosity of nanofluid and microorganisms by suspension, T_∞ denotes reference temperature, g denotes gravity vector,β denotes base fluid volumetric thermal expansion coefficient, $\Delta\rho = \rho_{\mathrm{cell}} - \rho_{\mathrm{bf}}$ denotes variations between densities of cell and base fluid, α denotes nanofluid thermal diffusivity, $\tau = (\rho c)_{\mathrm{p}}/(\rho c)_{\mathrm{f}}$ here $(\rho c)_p, (\rho c)_f$ denotes heat capacity of nanoparticles and fluid, respectively, D_{B} denotes coefficient of Brownian diffusion,D_{T} denotes coefficient of thermophoretic diffusion, $J = E + (V \times B)$, E is negligible by the reason of small Reynolds number, so, $J = (V \times B)$, $\sigma*$ denotes electrical conductivity of nanofluid, and K_l denotes chemical reaction coefficient. Identification is observed that the Oberbeck–Boussinesq limitation implemented to buoyancy force linearization in Eq. (2) by $\rho_{\mathrm{f}\infty}\beta(T - T_\infty)C$ was negligible. Dilute suspension nanoparticles consist this type of consideration so that the concept for gyrotactic microorganisms given by Pedley et al. [32] and Hill et al. [19] can be still utilizing here. Moreover, less temperature gradient through layer can ensure of the small that the alive microorganisms occurred in the fluid by suspension of nanoparticles.

Microorganisms flux j represented by (5) is defined as

$$j = N\bar{a} + N\hat{V} - D_n\nabla N, \tag{6}$$

Here $\hat{V} = (bW_{\mathrm{c}}/\Delta C)\nabla C$.

In that b denotes chemotaxis constant (m), D_n denotes microorganisms diffusivity, and W_{c} denotes swimming speed of maximum cell (m/s) (bW_{c} product taken as constant).

By the utilization of approximations of boundary layer, resultant equations above a vertical plate by a uniform free stream in the occurrence of nanoparticles and microorganisms [see Xu and Pop [45]] are as follows.

$$\left(\frac{\partial a_1}{\partial x}\right) + \left(\frac{\partial a_2}{\partial y}\right) = 0, \tag{7}$$

$$\rho_{\mathrm{f}}\left(\frac{\partial a_1}{\partial x}(a_1) + \frac{\partial a_1}{\partial y}(a_2)\right) - \sigma * B_0^2(a_1) = \frac{\partial^2 a_1}{\partial y^2}\upsilon + \left[\beta\,\rho_{\mathrm{f}\infty}(T - T_\infty)(1 - C_\infty) - (\rho_{\mathrm{p}} - \rho_{\mathrm{f}\infty})(C - C_\infty) + \gamma\,\Delta\rho N\right]g, \tag{8}$$

$$\left(\frac{\partial T}{\partial x}\right)(a_1) + \left(\frac{\partial T}{\partial y}\right)(a_2) - \frac{q'''}{\rho c_{\mathrm{p}}} - \alpha\frac{\partial^2 T}{\partial y^2} = \tau\left[D_{\mathrm{B}}\frac{\partial C}{\partial y}\frac{\partial T}{\partial y} + \frac{D_{\mathrm{T}}}{T_\infty}\left(\frac{\partial T}{\partial y}\right)^2\right], \tag{9}$$

$$\left(\frac{\partial C}{\partial x}\right)(a_1) + \left(\frac{\partial C}{\partial y}\right)(a_2) - \left(\frac{D_{\mathrm{T}}}{T_\infty}\right)\left(\frac{\partial^2 T}{\partial y^2}\right) = D_{\mathrm{B}}\frac{\partial^2 C}{\partial y^2}, \tag{10}$$

$$\left(\frac{\partial N}{\partial x}\right)(a_1) + \left(\frac{\partial N}{\partial y}\right)(a_2) + \frac{bW_{\mathrm{c}}}{C_{\mathrm{w}} - C_\infty}\left[\frac{\partial}{\partial y}\left(N\frac{\partial C}{\partial y}\right)\right] = D_n\frac{\partial^2 N}{\partial y^2}, \tag{11}$$

Boundary conditions

$$a_1 = \lambda u_{\mathrm{w}}(x),\ a_2 = 0,\ T = T_{\mathrm{f}},\ C = C_{\mathrm{w}},\ N = N_{\mathrm{w}},\ \text{at } y = 0, \tag{12}$$

$$a_1 \to 0,\ T \to T_\infty,\ C \to C_\infty,\ N \to N_\infty \text{ as } y \to \infty, \tag{13}$$

Here $\rho_{\mathrm{f}\infty}$ denotes base fluid density, C_∞ denotes reference concentration of nanoparticle, N_{w} denotes microorganisms concentration on the wall, T_{f} denotes temperature near the wall, λ denotes a constant with $\lambda = 0$ for a static (fixed) plate and $\lambda = 1$ for a dynamic (moving)

plate, k denotes nanofluid thermal conductivity. An internal heat generation/absorption q''' is modelled corresponding to given equations [30]

$$q''' = \frac{k}{x^2}\mathrm{Re}_x\left[a*(T_\mathrm{f}-T_\infty)e^{-\eta}+b*(T-T_\infty)\right] \tag{14}$$

First term of Eq. (14) denotes space coordinates dependence of the internal heat generation/absorption, while the end term of Eq. (14) denotes its dependence on the temperature. Also a^*, b^* denote temperature-dependent heat source/sink parameter and space-dependent heat source or sink parameter, respectively. Remember if the parameters $a^*>0$ and $b^*>0$, then situation will be heat generation internally, and if $a^*<0$ and $b^*<0$, then the situation will be internal heat absorption.

Use the following similarity transformations

$$\eta = \frac{y}{x}\mathrm{Ra}_x^{1/4},\ \ \psi = \alpha\mathrm{Ra}_x^{1/4}f(\eta),\ \ g(\eta)=\frac{T-T_\infty}{T_\mathrm{f}-T_\infty},\ \ h_1(\eta)=\frac{C-C_\infty}{C_\mathrm{w}-C_\infty},$$
$$h_2(\eta)=\frac{N-N_\infty}{N_\mathrm{w}-N_\infty},\ \ \mathrm{Ra}_x=\frac{(1-C_\infty)\beta g\Delta T_\mathrm{f}x^3}{\alpha\upsilon}, \tag{15}$$

Here $\psi(x, y)$ denotes stream function and satisfies automatically equation of mass conservation represented by (7). By the utilization of similarity transformation (15), velocity components take the form

$$a_1=\frac{\alpha}{x}\mathrm{Ra}_x^{1/2}f'(\eta),\ \ a_2=\frac{\alpha}{4}\mathrm{Ra}_x^{-3/4}f(\eta)+\alpha f'(\eta)\left[\frac{\eta}{4}Ra_x^{-3/4}-\frac{\eta}{x}Ra_x^{1/4}\right], \tag{16}$$

As well as governing Eqs. (8)–(11) are transmitted into

$$f'''+\frac{1}{4\,\mathrm{Pr}}\left(3f''f-2f'^2\right)-Mf'+g-\mathrm{Nr}\,h_1-\mathrm{Rb}\,h_2=0, \tag{17}$$

$$g''+\frac{3}{4}fg'+\mathrm{Nb}\,h_1'g'+\mathrm{Nt}\,g'^2+(a*e^{-\eta}+b*g)=0, \tag{18}$$

$$h_1''+\frac{3}{4}\mathrm{Le}\,f\,h_1'+\frac{\mathrm{Nt}}{}\mathrm{Nb}g''=0, \tag{19}$$

$$h_2''+\frac{3}{4}\mathrm{Lb}\,f\,h_2'-\mathrm{Pe}\left[h_1'h_2'+h_1''(\sigma+h_2)\right]=0, \tag{20}$$

The corresponding dimensionless boundary conditions are

$$f(0)=0,\ f'(0)=\lambda,\ g(0)=1,\ h_1(0)=1,\ h_2(0)=1, \tag{21}$$

$$f'(\infty)=0,\ g(\infty)=0,\ h_1(\infty)=0,\ h_2(\infty)=0, \tag{22}$$

where $f'(\eta)$ denotes nondimensional velocity, $g(\eta)$ denotes nondimensional temperature distribution, $h_1(\eta)$ denotes concentration of nondimensional nanoparticles, $h_2(\eta)$ denotes nondimensional density of motile microorganisms, M denotes magnetic field parameter, σ denotes bioconvection constant, Le denotes traditional Lewis number, Lb denotes bioconvection Lewis number, Pe denotes bioconvection Péclet number, Rb denotes bioconvection Reynolds number, Nt denotes thermophoretic parameter, Nb denotes Brownian motion parameter, Nr denotes buoyancy ratio parameter, Pr denotes Prandtl number and defined by

$$M=\frac{\sigma B_0^2x^2}{\upsilon\rho_\mathrm{f}Ra_x^{1/2}},\ \ \sigma=\frac{N_\mathrm{w}}{\Delta N_\mathrm{w}},\ \ \mathrm{Le}=\frac{\alpha}{D_\mathrm{B}},\ \ \mathrm{Lb}=\frac{\alpha}{D_n},\ \ \mathrm{Pe}=\frac{bW_\mathrm{c}}{D_n},$$
$$\mathrm{Rb}=\frac{\gamma\Delta N_\mathrm{w}\Delta\rho}{\rho_\mathrm{f}\beta(1-C_\infty)\Delta T_\mathrm{f}},\ \ \mathrm{Nt}=\frac{\tau D_\mathrm{T}\Delta T_\mathrm{f}}{\alpha T_\infty},\ \ \mathrm{Nb}=\frac{\tau D_\mathrm{B}\Delta C_\mathrm{w}}{\alpha},$$

$$\mathrm{Nr} = \frac{(\rho_p - \rho_f)\Delta C_w}{\rho_f(1 - C_\infty)\beta\Delta T_f}, \ \mathrm{Pr} = \frac{\upsilon}{\alpha}. \tag{23}$$

Physical quantities of local skin friction coefficient C_{fx}, local Nusselt number Nu_x, local wall mass flux Q_{mx}, local wall motile microorganisms flux Q_{nx} are described as

$$C_{fx} = \frac{\tau_w}{\rho_f u_w^2}, \ Nu_x = \frac{xq_w}{k(T_f - T_\infty)}, \ Q_{mx} = \frac{xq_m}{D_B(C_w - C_\infty)}, \ Q_{nx} = \frac{xq_n}{D_n(N_w - N_\infty)}, \tag{24}$$

here $\tau_w = \mu\left(\frac{\partial a_1}{\partial y}\right)_{y=0}$, $q_w = -k\left(\frac{\partial T}{\partial y}\right)_{y=0}$, $q_m = -D_B\left(\frac{\partial C}{\partial y}\right)_{y=0}$, $q_n = -D_n\left(\frac{\partial N}{\partial y}\right)_{y=0}$.

Substituting similarity transformation (15) in Eq. (24), we acquire

$$\begin{aligned} Cfr &= \mathrm{Ra}_x^{-1/4} C_{fx} = f''(0), \\ Nur &= \mathrm{Ra}_x^{1/4} \mathrm{Nu}_x = -g'(0), \\ Shr &= \mathrm{Ra}_x^{1/4} Q_{mx} = -h_1'(0), \\ Xnr &= \mathrm{Ra}_x^{1/4} Q_{nx} = -h_2'(0). \end{aligned} \tag{25}$$

where the local Rayleigh number $\mathrm{Ra}_x = \frac{(1-C_\infty)\beta g \Delta T_f}{\alpha \upsilon x^3}$.

3 Method of solution

By the help of effective computational spectral relaxation method (SRM), we solved ordinary differential equations represented from (16) to (19) together with boundary conditions represented by (20), (21) and they transmitted into group of ordinary differential equations which are linear. By the help of SRM, we evaluated numerical values of temperature, fluid velocity, nanoparticles concentration, motile microorganisms density, local skin friction, local Nusselt and Sherwood numbers and local wall motile microorganism flux. Assume a group of m ordinary differential equations which are nonlinear in m unknown functions, $z_i(\eta)$, $i = 1, 2, \ldots m$ here $\eta \in [a, b]$ denotes independent variable taken to start powerful tool SRM algorithm. Such iterative scheme is solved by using Chebyshev pseudospectral method, and detailed facts can be found by Canuto et al. [6] and Trefethen [43]. To apply the SRM technique it is necessary to decrease the order of nonlinear ordinary differential equations. By using $f' = q$, group of nonlinear equations transforms into the following set of equations:

$$f' = q, \tag{26}$$

$$q'' + \frac{1}{4\,\mathrm{Pr}}\left(3\,f\,q' - 2q^2\right) - M\,q + g - \mathrm{Nr}\,h_1 - \mathrm{Rb}\,h_2 = 0, \tag{27}$$

$$g'' + \frac{3}{4} f\,g' + \mathrm{Nb}\,h_2'\,h_1' + \mathrm{Nt}\,g'^2 + (a * e^{-\eta} + b * g) = 0, \tag{28}$$

$$h_1'' + \frac{3}{4}\mathrm{Le}\,f\,h_1' + \frac{\mathrm{Nt}}{}\mathrm{Nb}g'' = 0, \tag{29}$$

$$h_2''\frac{3}{4}\mathrm{Lb}\,f\,h_2' - \mathrm{Pe}\left[h_1'\,h_2' + h_1''\,(\sigma + h_2)\right] = 0, \tag{30}$$

By the substitution, boundary constraints are altered as

$$f(0) = 0, \ q(0) = \lambda, \ g(0) = 1, \ h_1(0) = 1, \ h_2(0) = 1, \tag{31}$$

$$q(\infty) = 0,\ g(\infty) = 0,\ h_1(\infty) = 0,\ h_2(\infty) = 0. \tag{32}$$

This algorithm works with Gauss–Seidel approach to decouple system of governing equalities represented from (25) to (29). In the process of SRM technique on (25)–(29) the iteration scheme results in the following linear partial differential equations.

$$f'_{r+1} = q_{r+1}, \qquad f_{r+1}(0) = 0, \tag{33}$$

$$q''_{r+1} + \frac{1}{4\,\mathrm{Pr}}\left(3\,f_{r+1}\,q'_{r+1} - 2q^2_{r+1}\right) - M\,q_{r+1} + g_{r+1} - \mathrm{Nr}\,(h_1)_{r+1} - \mathrm{Rb}\,(h_2)_{r+1} = 0,$$
$$q_{r+1}(0) = \lambda,\ \ q_{r+1}(\infty) = 0, \tag{34}$$

$$g''_{r+1} + \frac{3}{4} f_{r+1}\,g'_{r+1} + \mathrm{Nb}\,(g')_{r+1}\,(h'_1)_{r+1} + \mathrm{Nt}\,g'^2_{r+1} + (a * e^{-\eta} + b * g_{r+1}) = 0,$$
$$g_{r+1}(0) = 1,\ \ g_{r+1}(\infty) = 0, \tag{35}$$

$$(h''_1)_{r+1} + \frac{3}{4}\mathrm{Le}\,f_{r+1}\,(h'_1)_{r+1} + \frac{Nt}{Nb} g'_{r+1} = 0,$$
$$(h_1)_{r+1}(0) = 1, \quad (h_1)_{r+1}(\infty) = 0, \tag{36}$$

$$(h''_2)_{r+1\ r+1} + \frac{3}{4}\mathrm{Lb}\,f_{r+1}\,(h'_2)_{r+1} - \mathrm{Pe}\left[(h'_1)_{r+1}\,(h'_2)_{r+1} + (h''_1)_{r+1}\,(\sigma + (h_2)_{r+1})\right] = 0,$$
$$(h_2)_{r+1}(0) = 1,\ \ (h_2)_{r+1}(\infty) = 0, \tag{37}$$

To apply spectral method, domain is altered to the interval $[-1, 1]$ by the transformation $\eta = \eta_\infty(Y + 1)/2$. The necessary thought to apply the spectral collocation method is to evaluate differentiation matrix $\mathcal{D}$ and utilized to estimate derivatives of not known variables of (η) near collocation points (grid points) in terms of product of matrix vector

$$\frac{\mathrm{d}f}{\mathrm{d}\eta} = \sum_{k=0}^{N_x} D_{j\,k}\,f(\eta_k) = Df, \quad j = 0,\ 1,\ 2,\ \ldots,\ N_x, \tag{38}$$

In the above $N_x + 1$ represents number of collocation points, $f = \left[f(Y_0),\ f(Y_1), \ldots f\left(Y_{N_x}\right)\right]^{\mathrm{T}}$ denotes vector function at the collocation points and $\boldsymbol{D} = \frac{2\mathcal{D}}{\eta_\infty}$: Higher-order derivatives are attained in powers of $\boldsymbol{D}$ like

$$f^{(p)} = \boldsymbol{D}^p\,f, \tag{39}$$

Here derivative order is denoted as p. Nodes are defined by using Gauss–Lobatto collocation points in the interval $[-1, 1]$ defined as

$$Y_j = \cos\left(\frac{\pi_j}{N_x}\right), \qquad j = 0,\ 1,\ 2,\ \ldots N_x, \tag{40}$$

$(N_x + 1) \times (N_x + 1)$ is the size of matrix $\boldsymbol{D}$, and total number of grid points is represented by $N_x + 1$ in the η direction.

$$A_1\,\boldsymbol{f}_{r+1} = B_1, \qquad f_{r+1}(Y_{N_x}) = 0, \tag{41}$$

$$A_2\,\boldsymbol{q}_{r+1} = B_2, \qquad q_{r+1}(Y_{N_x}) = \lambda, \quad q_{r+1}(Y_0) = 0, \tag{42}$$

$$A_3\,\boldsymbol{g}_{r+1} = B_2, \qquad g_{r+1}(Y_{N_x}) = 1, \quad g_{r+1}(Y_0) = 0, \tag{43}$$

$$A_4\,(\boldsymbol{h_1})_{r+1} = B_4, \qquad (h_1)_{r+1}(Y_{N_x}) = 1, \quad (h_1)_{r+1}(Y_0) = 0, \tag{44}$$

$$A_5\,(\boldsymbol{h_2})_{r+1} = B_5, \qquad (h_2)_{r+1}(Y_{N_x}) = 1, \quad (h_2)_{r+1}(Y_0) = 0, \tag{45}$$

where

$$A_1 = \boldsymbol{D}, \qquad B_1 = q_{r+1}, \tag{46}$$

$$A_2 = \boldsymbol{D}^2 + \mathrm{diag}\left[\frac{3}{4\,\mathrm{Pr}}\,f_{r+1}\right]\boldsymbol{D} - M\,\boldsymbol{I}, \qquad B_2 = \frac{1}{2\,\mathrm{Pr}}q_{r+1}^2, \tag{47}$$

$$A_3 = \boldsymbol{D}^2 + \mathrm{diag}\left[\frac{3}{4}\,f_{r+1} + \mathrm{Nb}\,(\boldsymbol{h_1'})_{r+1}\right]\boldsymbol{D} + b * \boldsymbol{I},$$

$$B_3 = -\mathrm{Nt}\,\boldsymbol{g}_{r+1}'^2 - a * e^{-\eta}, \tag{48}$$

$$A_4 = \boldsymbol{D}^2 + \mathrm{diag}\left[\frac{3}{4}\,f_{r+1}\right]\boldsymbol{D}, \qquad B_4 = -\frac{Nt}{Nb}\,\boldsymbol{g}_{r+1}'', \tag{49}$$

$$A_5 = \boldsymbol{D}^2 + \mathrm{diag}\big[\mathrm{Lb}\,f_{r+1} - \mathrm{Pe}\,(\boldsymbol{h_1'})_{r+1}\big]\boldsymbol{D} - \mathrm{Pe}\,(\boldsymbol{h_1''})_{r+1}, \qquad B_5 = \mathrm{Pe}\,\sigma\,(\boldsymbol{h_1''})_{r+1}, \tag{50}$$

In Eqs. (47)–(50), identity matrix and diagonal matrix are denoted by I and diag[], $\boldsymbol{f}$, $\boldsymbol{q}$, $\boldsymbol{g}$, $\boldsymbol{h_1}$ and $\boldsymbol{h_2}$ represent values of f, q, g, h_1 and h_2 functions correspondingly, when evaluated near grid points, and iteration number is denoted by subscript r.

To Eqs. (41)–(45), we are utilizing the following functions as first guess to begin SRM scheme and boundary conditions satisfied by these initial guesses. To physical consideration, velocity profile, temperature profile, nanoparticles concentration profile and density motile microorganism profile to the boundary layer problem are analysed in this work at $\eta = \infty$.

$$f_0(\eta) = \lambda\big(1 - e^{-\eta}\big), \quad q_0(\eta) = \lambda e^{-\eta}, \quad g_0(\eta) = e^{-\eta}, \quad (h_1)_0(\eta) = e^{-\eta}, \quad (h_2)_0(\eta) = e^{-\eta} \tag{51}$$

This process is continuously repeated until convergence is reached. An infinity norm is used to represent SRM scheme convergence and is depicted as

$$\mathrm{Er} = \mathrm{Max}(\|f_{r+1} - f_r\|, \ \|q_{r+1} - q_r\|, \ \|g_{r+1} - g_r\|, \ \|(h_1)_{r+1} - (h_1)_r\|, \ \|(h_2)_{r+1} - (h_2)_r\|) \tag{52}$$

Exactness of this method is identified by escalating collocation point number N_x up to the consistent solutions, and change in the solution does not exist by the raising values of collocation points.

4 Results and discussion

By the utilization of SRM, system of equations represented from (16) to (19) together boundary conditions represented from (20) to (21) is solved numerically. SRM is a new scheme and it is suggested by Motsa [31]. Numerical simulations are done to estimate the numerical results of the physical quantities, namely surface shear stress, surface mass transfer, surface heat transfer and motile microorganisms' density. In the spectral method, a finite computational domain of extent $\eta_\infty = 50$ is preferred in the direction of η. With the help of numerical experimentation η is identified to provide exact results to all governing physical quantities. By numerical technique we determine that $N_x = 120$ grid points which give spectral relaxation method with sufficient accuracy. In fact, SRM is iterative scheme. In this study tolerance level is considered as $\varepsilon = 10^{-9}$. Consider the nondimensional parameter values as $\mathrm{Pr} = 6.2$, $M = 0.5$, $\mathrm{Nr} = 0.2$, $\mathrm{Nt} = 0.1$, $\mathrm{Rb} = 0.2$, $\mathrm{Nb} = 0.1$, $\mathrm{Le} = 1$, $\mathrm{Lb} = 2$, $\mathrm{Pe} = 1$, $\sigma = 0.2$, $a^* = 0.1$, and $b^* = 0.1$ to the numerical results. Throughout the study these values are kept as

Table 1 Comparison of the present SRM solutions with the previously published data in the absence of nanofluid and bioconvection parameters

Pr	Nur					
	Bejan [3]	Rosca et al. [37]	Kuznetsov and Nield [26]	Khan et al. [23]	Present results (SRM)	Present results (bvp4c)
0.01	0.162	0.180	–	–	0.18021197	0.18021197
0.72	0.387	0.387	–	–	0.38737229	0.38737229
1	0.401	0.401	0.401	0.40135	0.40103314	0.40103314
2	0.426	0.426	–	–	0.42601367	0.42601367
10	0.465	0.464	0.449	0.46903	0.46496852	0.46496852
100	0.490	0.489	0.458	0.49260	0.48995167	0.48995167
1000	0.499	0.497	0.459	0.49878	0.49770566	0.49770566

common excluding the variations in corresponding figures and tables. Comparison of SRM, bvp4c and previous results is shown in Tables 1, 2 and 3. From these tables a lot of confidence existed to us to find the results. Variations of heat transfer to raising values of Prandtl number quantity are shown in Table 1. Also, heat transfer rate near surface rises by the accelerating values of Prandtl number. We built up the precision of the spectral relaxation strategy by contrasting the SRM results and those acquired utilizing the MATLAB bvp4c solver. The correlation in Tables 2 and 3 shows a decent understanding between the two techniques, and this examination gives a benchmark to gauge the precision and productivity of the strategy.

From these tables, we observed that Cfr is improved by 333.87% for raising values of magnetic parameter quantity M from 0.3 to 1.0, whereas Nu_r, Sh_r and Xn_r are reduced by 29.02%, 11.91% and 8.83% correspondingly, so that reason frictional drag increases between the layers of fluid, and as a result, decrement of transmission of heat and mass transfer is observed when the value of M increases. Also, noticed that the self-swimming microorganism flux rate decreases. When Nt enlarges from 0.1 to 0.5, Cf_r is increased by 86.87% and Nu_r, Sh_r and Xn_r are reduced by 34.63%, 425.87% and 44.87%, respectively, with the existence of various parameters. It is concluded that in both heat and mass transfer rate, motile microorganism flux decreases, whereas increases the surface shear rate with increase in Nt. By the increase of Nb from 0.1 to 0.5,Cf_r is decreased by 100.05% and Nu_r is reduced by 26.0%, whereas Sh_r and Xn_r are improved by 42.29% and 12.93%, respectively. Another observation identified that the lower elements of Nb, Cf_r and Nu_r take the higher elements and the reason is nanofluid viscosity raises as Nb raises which in turn decreases the surface shear stress and rate of transport of heat transfer, but it shows an opposite behaviour to mass transfer rate and motile microorganism flux. In practical applications, the flow drag in the boundary layer is reduced gradually as nanoparticles are continuously added into the base fluids. The higher values of $a*$ from $-$ 0.3 to 1.4 give a nonpositive effect on skin friction coefficient, i.e. Cf_r decreased by 618.19% and Nu_r by 254.26%, and positive impact on other physical quantities, i.e. it enhanced Sh_r by 182.96% and Xn_r by 44.58%. An impact of $b*$ is observed in Tables 2 and 3. As $b*$ enlarges from $-$ 0.2 to 0.3, Cf_r is reduced by 2246.02%, Nu_r is decelerated by 303.8%, Sh_r is increased by 209.36%, and Xn_r is enlarged by 48.15%, respectively.

Figure 2 and 3 show the stream lines in the flow region about magnetic field strength $M = 0.5$ and $M = 2$. Streams lines are very near to stagnation point $x = 0$ in the case of low strength of magnetic field, but opposite results are occurred in higher magnetic field strength.

Table 2 Comparison of SRM solutions with bvp4c for Cfr and Nur

M	Nt	b	a*	b*	Bvp 4c CPU time in sec	SRM CPU time in sec	SRM Cfr	Bvp4c Cfr	SRM Nur	Bvp4c Nur
0.3	0.1	0.1	0.1	0.1	3.020450	1.517541	0.14274806	0.14274806	0.43072709	0.43072709
0.6					3.470973	1.808697	0.37592853	0.37592853	0.38385366	0.38385366
0.8					3.246986	1.651690	0.50448828	0.50448828	0.35756078	0.35756078
1.0					3.336965	1.667671	0.61933188	0.61933188	0.33385660	0.33385660
	0.2				3.528744	1.684339	0.17401984	0.17401984	0.40345663	0.40345663
	0.3				3.847209	1.782431	0.20477075	0.20477075	0.37638194	0.37638194
	0.4				4.029485	1.786088	0.23540399	0.23540399	0.34897223	0.34897223
	0.5				4.332209	3.451951	0.26678236	0.26678236	0.31997118	0.31997118
		0.2			3.336181	1.640825	0.11210414	0.11210414	0.41091811	0.41091811
		0.3			3.399712	1.804641	0.09565808	0.09565808	0.38779129	0.38779129
		0.4			4.912170	1.847506	0.08277555	0.08277555	0.36457084	0.36457084
		0.5			3.622290	1.652513	0.07136758	0.07136758	0.34186769	0.34186769
			− 0.2		4.360378	1.925485	0.23527677	0.23527677	0.62570312	0.62570312
			− 0.1		3.311806	1.493753	0.20315539	0.20315539	0.56017971	0.56017971
			0.2		3.957953	1.785520	0.11407738	0.11407738	0.36666689	0.36666689
			0.3		3.331219	1.918249	0.08625050	0.08625050	0.30298716	0.30298716
			0.4		3.251001	2.244088	0.05916989	0.05916989	0.23965157	0.23965157
			0.5		3.321750	2.431800	0.03275695	0.03275695	0.17662997	0.17662997
				− 0.2	3.348891	1.097352	0.24101419	0.24101419	0.64372083	0.64372083
				− 0.1	3.206599	1.509177	0.21134047	0.21134047	0.57767750	0.57767750
				0.2	3.403698	2.030137	0.10297812	0.10297812	0.34813624	0.34813624
				0.25	3.328293	4.008966	0.08152712	0.08152712	0.30412309	0.30412309
				0.3	3.873551	3.625679	0.05895653	0.05895653	0.25810674	0.25810674
				0.4	3.411146	3.648499	0.01027150	0.01027150	0.15941638	0.15941638

Table 3 Comparison of SRM solutions with bvp4c for *Shr* and *Xnr*

M	Nt	Nb	*a**	*b**	SRM *Shr*	Bvp4c *Shr*	SRM *Xnr*	Bvp4c *Xnr*
0.3	0.1	0.1	0.1	0.1	0.43892574	0.43892574	1.28883776	1.28883776
0.6					0.41310050	0.41310050	1.23528011	1.23528011
0.8					0.40122825	0.40122825	1.20762248	1.20762248
1.0					0.39226153	0.39226153	1.18427992	1.18427992
	0.2				0.26709952	0.26709952	1.15366645	1.15366645
	0.3				0.11894896	0.11894896	1.04698110	1.04698110
	0.4				− 0.01157404	− 0.01157404	0.96213694	0.96213694
	0.5				− 0.13468810	− 0.13468810	0.88965325	0.88965325
		0.2			0.55272036	0.55272036	1.38857715	1.38857715
		0.3			0.59172282	0.59172282	1.42406412	1.42406412
		0.4			0.61190236	0.61190236	1.44312788	1.44312788
		0.5			0.62452289	0.62452289	1.45554859	1.45554859
			− 0.2		0.24202079	0.24202079	1.07566960	1.07566960
			− 0.1		0.30929048	0.30929048	1.14849044	1.14849044
			0.2		0.50182325	0.50182325	1.35694670	1.35694670
			0.3		0.56368277	0.56368277	1.42394596	1.42394596
			0.4		0.62463472	0.62463472	1.48997997	1.48997997
			0.5		0.68478312	0.68478312	1.55516417	1.55516417
				− 0.2	0.22609239	0.22609239	1.05901843	1.05901843
				− 0.1	0.29278415	0.29278415	1.13114216	1.13114216
				0.2	0.51956501	0.51956501	1.37565666	1.37565666
				0.25	0.56207496	0.56207496	1.42137155	1.42137155
				0.3	0.60617094	0.60617094	1.46875550	1.46875550
				0.4	0.69952719	0.69952719	1.56895338	1.56895338

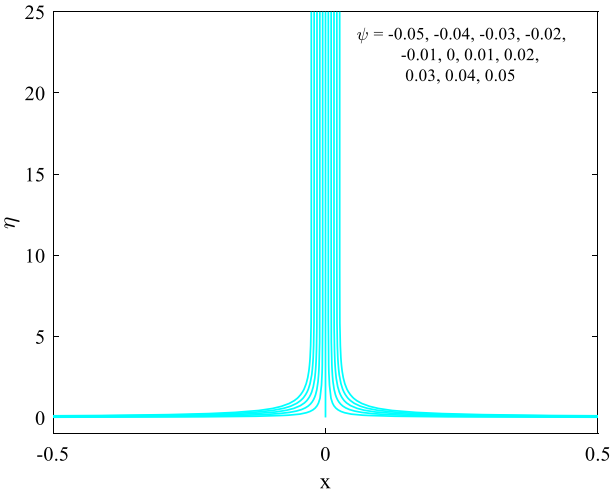

Fig. 2 Streamlines for $M = 0.5$

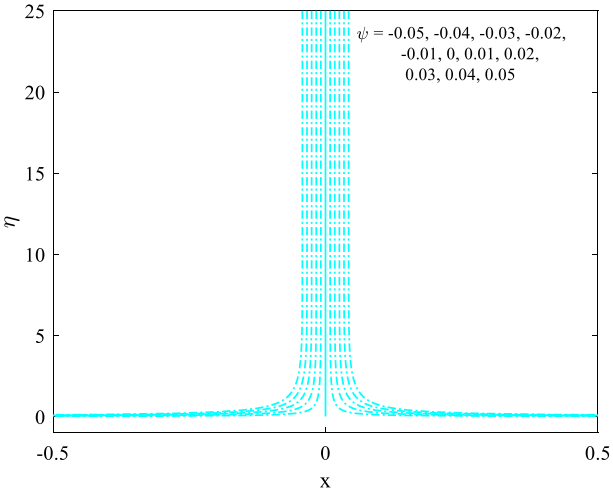

Fig. 3 Streamlines for $M = 2$

Figure 4 exhibits that velocity component $f'(\eta)$ decreases for the increasing values of magnetic field strength M and bioconvection Reynolds number Rb. The physical reason is that for raising values of magnetic field M, there exists a drag force between the fluid layers which is called "Lorentz force". As a result, fluid velocity goes down. The same result is reflected in Table 2 also. Moreover, here working fluid is electrically conducted, nanosolid particles are moving within the fluid medium, so that particles are influenced by magnetic flux. By all these effects, fluid velocity falls down as observed in Fig. 4.

Figure 5 explains about the profiles of temperature for varying values of magnetic field strength M. Observation from this figure is that enhancement in the temperature is noted due to the effect of M. Due to the Lorentz force which is caused by magnetic field effect, friction is developed among fluid layers. Because of this friction, fluid particles are getting heated. As

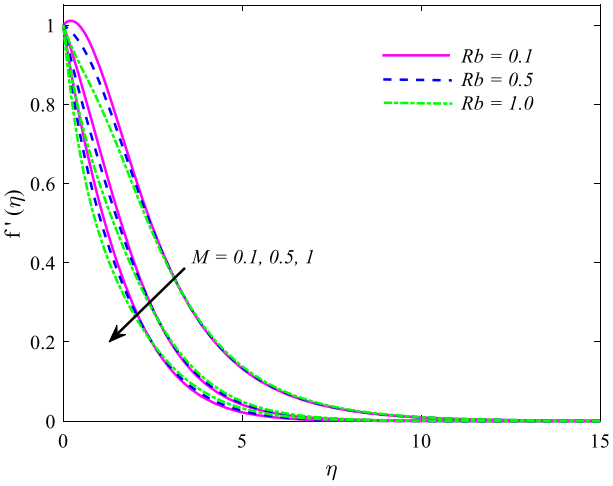

Fig. 4 Velocity distribution $f'(\eta)$ verses M to distinct values of Rb

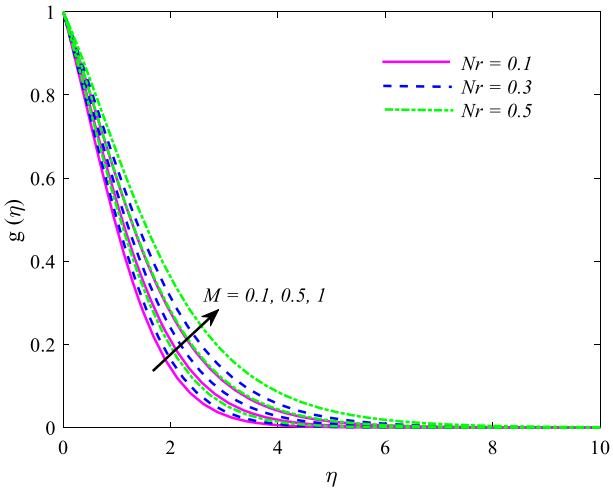

Fig. 5 Temperature distribution $g(\eta)$ verses M to distinct values of Nr

a result, temperature profile increases as shown in Fig. 5. Also, Fig. 5 reflects enhancement in the temperature profile for the increasing of buoyancy ratio parameter.

Figure 6 demonstrates the effects of heat generation/absorption parameters a^* and b^* on temperature distribution by taking remaining parameters as fixed value. Temperature profile and thermal boundary layer thickness become very strong with the raising values of internal heat generation parameters $a^*>0$ and $b^*>0$, but opposite effects are observed for heat absorption parameters $a^*<0$ and $b^*<0$. Moreover, heat transfer rate is decreased in case of heat generation parameters and an opposite trend is observed in case of heat absorption parameters.

Temperature and nanoconcentration profiles can be observed from Figs. 7 and 8 for the two important impacts that is Brownian motion Nb and thermophoretic parameter Nt. Here, it is found that, for increasing estimations of Nb, temperature distribution is enhanced, and

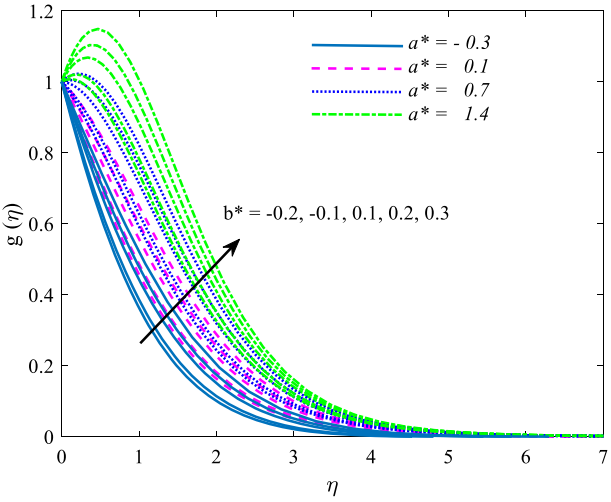

Fig. 6 Temperature distribution $g(\eta)$ verses $b*$ to distinct values of $a*$

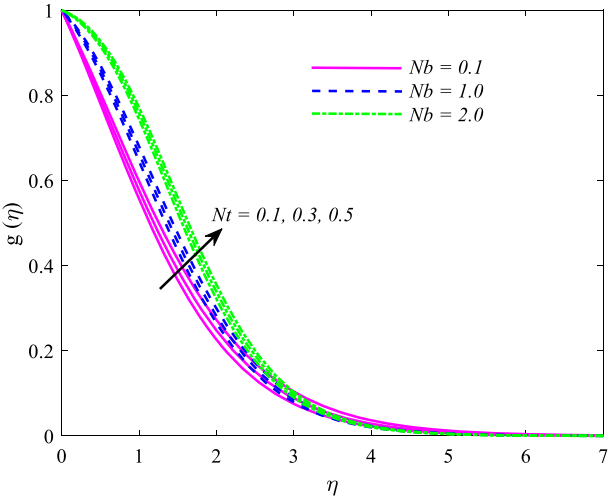

Fig. 7 Temperature distribution $g(\eta)$ verses Nt to distinct values of Nb

now coming to concentration profile, it is reduced as presented in Figs. 7 and 8. Further, these two profiles are increased for the raising Nt. Reason behind this is that temperature gradient produces thermophoretic force and this force generates a high-speed flow away from the vertical plate. Moreover, thermal boundary layer thickness rises with escalating of Nt. This physical behaviour is in good agreement with those of Mahdy [27], Xu and Pop [45].

Concentration profile based on Lewis number Le and magnetic field M is exhibited in Fig. 9. Nanoparticle volume fraction decreases along with the larger values of Le, and Le is defined as proportion of thermal and mass diffusivity. Thickness of thermal boundary layer increases, and thickness of concentration boundary layer decreases for the rising values of Le. Also identified one more point is that the nanoconcentration profile rises to rising values

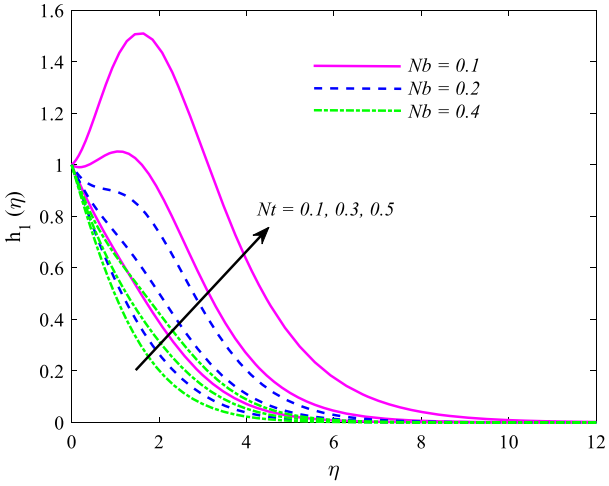

Fig. 8 Concentration distribution $h_1(\eta)$ verses Nt to distinct values of Nb

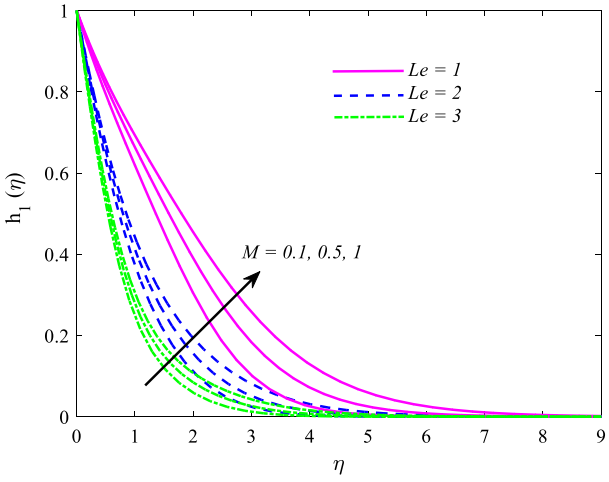

Fig. 9 Concentration distribution $h_1(\eta)$ verses M to distinct values of Le

of M. Physics behind is that the nanosolid particles are attracted towards the boundary layer by the increasing of magnetic flux. So, the concentration profile escalated.

Variations in profiles of motile microorganisms against Lewis bioconvection number and various values of magnetic field are displayed in Fig. 10. Microorganisms profile rises by the rising values of magnetic parameter, whereas the bioconvection Lewis number decreases profiles of microorganisms. The bioconvection Lewis number plays similar nature as regular Lewis number.

An impact of Péclet number Pe and bioconvection constant σ on the nondimensional motile microorganisms is displayed in Fig. 11. It is making sure that an increase in Pe decreases the density of microorganisms. Effect of σ is similar as Pe on motile microorganisms' density.

The current analysis has offered some insight into Brownian motion and thermophoresis effects on the motion of magnetohydrodynamic nanofluid in bioconvection boundary layer flow with heat generation/absorption. The computations may be relevant to materials processing of biofuel cells. Attention has been confined to Newtonian viscous base fluids, and the free convection on non-Newtonian nanofluid has been ignored.

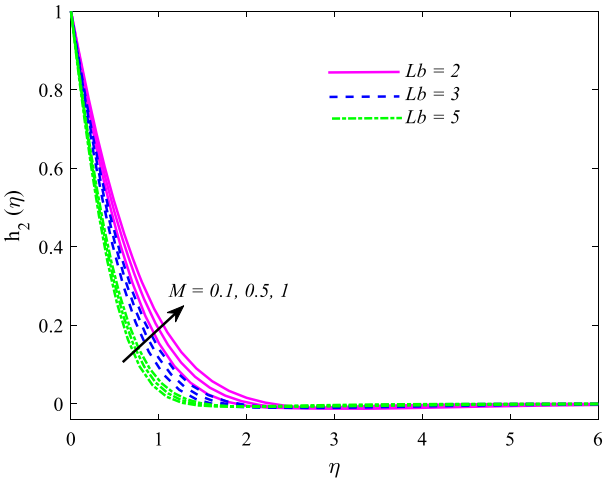

Fig. 10 Motile microorganism density distribution $h_2(\eta)$ verses M to distinct values of Lb

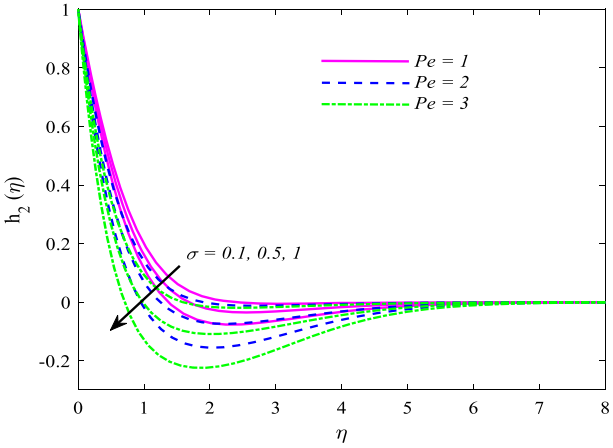

Fig. 11 Motile microorganism density distribution $h_2(\eta)$ verses σ to distinct values of Pe

Finally, the outcomes show that the SRM is exact and adequately vigorous for use in taking care of fluid flow problems and as an option in contrast to the already available methods like Runge–Kutta, Keller box and so on in finding solutions of boundary layer equations.

5 Conclusions

The natural convective boundary layer flow about a vertical plate in bioconvection of a nanofluid comprising gyrotactic microorganisms in existence of a magnetic field and heat generation/absorption effects has been examined numerically in detail, and the impacts of Brownian motion and thermophoresis are involved in the model for nanofluids. The obtained outcomes are exhibited graphically and analysed qualitatively by varying the controlling parameters.

A few conclusions obtained with this study are mentioned below.

1. The outcomes reveal that, in the heat and mass transfer, the motile microorganism flux rates and the momentum boundary layer thickness are decreased throughout the fluid medium as a result of increasing the magnetic parameter M.
2. The drag stress rate, temperature distribution and the motile microorganism profiles are enhanced with M.
3. The reduced Nusselt number decreases with rising values of the Brownian motion and the thermophoresis effect, but it increases for the bioconvection Péclet number.
4. The Sherwood numbers increase with the increase of the Brownian motion and the bioconvection Péclet number.
5. The heat transfer rate reduces with the heat generation parameter increments, whereas the fluid heat transfer rate rises with higher values of the heat absorption parameter.
6. Temperature profile is enhanced for the increasing values of buoyancy ratio parameter.
7. Temperature profile and thermal boundary layer thickness become very strong with the raising values of internal heat generation parameters, but opposite effects are observed for heat absorption parameters.
8. Concentration profile decreases for the rising values of Lewis number, whereas it rises for rising values of magnetic parameter.
9. It is found that for increasing estimations of Brownian motion parameter, temperature distribution is enhanced and concentration profile is reduced. Further, these two profiles are increased for the raising thermophoretic parameter.

References

1. A.I. Alsabery, I. Hashim, A. Hajjar, M. Ghalambaz, S. Nadeem, M. Saffari Pour, Entropy generation and natural convection flow of hybrid nanofluids in a partially divided wavy cavity including solid blocks. Energies **13**, 2942 (2020)
2. A. Aziz, W.A. Khan, I. Pop, Free convection boundary layer flow past a horizontal flat plate embedded in porous medium filled by nanofluid containing gyrotactic microorganisms. Int. J. Therm. Sci. **56**, 48–57 (2012)
3. A. Bejan, *Convection Heat Transfer*, 2nd edn. (Wiley, New York, 1995)
4. J. Buongiorno, Convective transport in nanofluids. ASME J. Heat Transf. **128**, 240–250 (2006)
5. J. Buongiorno, W. Hu, Nanofluid coolants for advanced nuclear power plants. Paper No. 5705, *Proceedings of ICAPP'05, Seoul, May 15–19* (2005)
6. C. Canuto, M.Y. Hussaini, A. Quarteroni, T.A. Zang, *Spectral Methods in Fluid Dynamics* (Springer, Berlin, 1988)
7. T. Chakraborty, K. Das, K. Prabir Kumar, Framing the impact of external magnetic field on bioconvection of a nanofluid flow containing gyrotactic microorganisms with convective boundary conditions. Alex. Eng. J. **57**, 61–71 (2018)
8. H. Chen, J. Chen, Y. Geng, K. Chen, K. Chen, Three-dimensional boundary layer flow over a rotating disk with power law stretching in a nanofluid containing gyrotactic microorganisms. Heat Transf. Asian Res. **47**(3), 569–582 (2018)
9. W. Duangthongsuk, S. Wongwises, Effect of thermophysical properties models on the predicting of the convective heat transfer coefficient for low concentration nanofluid. Int. Commun. Heat Mass Transf. **35**(10), 1320–1326 (2008)
10. K. Ganesh Kumar, B.J. Gireesha, S. Manjunatha, N.G. Rudraswamy, "Effect of nonlinear thermal radiation on double-diffusive mixed convection boundary layer flow of viscoelastic nanofluid over a stretching sheet. Int. J. Mech. Mater. Eng. **12**, 18 (2017)
11. K. Gangadhar, T. Kannan, P. Jayalakshmi, Magnetohydrodynamic micropolar nanofluid past a permeable stretching/shrinking sheet with Newtonian heating. J. Braz. Soc. Mech. Sci. Eng. **39**, 4379–4391 (2017)
12. K. Gangadhar, T. Kannan, G. Sakthivel, K. Dasaradha Ramaiah, Unsteady free convective boundary layer flow of a nanofluid past a stretching surface using a spectral relaxation method. Int. J. Ambient Energy **41**(6), 609–616 (2020)

13. K. Gangadhar, K. Keziya, S.M. Ibrahim, Effect of thermal radiation on engine oil nanofluid flow over a permeable wedge under convective heating: Keller box method. Multidiscip. Model. Mater. Struct. **15**(1), 187–205 (2019)
14. K. Gangadhar, N.S.L.V. Narasimharao, B. Satyanarayana, Thermal diffusion and viscous dissipation effects on heat and mass filled with TiO_2 and Al_2O_3 water based nanofluids. Comput. Therm. Sci. **11**(6), 523–539 (2019)
15. P. Geng, A.V. Kuznetsov, Introducing the concept of effective diffusivity to evaluate the effect of bioconvection on small solid particles. Int. J. Transp. Phenom. **7**, 321–338 (2005)
16. M. Ghalambaz, T. Grosan, I. Pop, Mixed convection boundary layer flow and heat transfer over a vertical plate embedded in a porous medium filled with a suspension of nano-encapsulated phase change materials. J. Mol. Liq. **293**, 111432 (2019)
17. S. Ghorai, N.A. Hill, Development and stability of gyrotactic plumes in bioconvection. J. Fluid Mech. **400**, 1–31 (1999)
18. A. Hajjar, S.A.M. Mehryan, M. Ghalambaz, Time periodic natural convection heat transfer in a nano-encapsulated phase—change suspension. Int. J. Mech. Sci. **166**, 105243 (2020)
19. N.A. Hill, T.J. Pedley, J.O. Kessler, Growth of bioconvection patterns in a suspension of gyrotactic microorganisms in a layer of finite depth. J. Fluid Mech. **208**, 509–543 (1989)
20. T. Ishikawa, Suspension biomechanics of swimming microbes. J. R. Soc. Interface **6**(39), 815–834 (2009)
21. W.A. Khan, O.D. Makinde, MHD nanofluid bioconvection due to gyrotactic microorganisms over a convectively heat stretching sheet. Int. J. Therm. Sci. **81**, 118–124 (2014)
22. W.A. Khan, I. Pop, Boundary-layer flow of a nanofluid past a stretching sheet. Int. J. Heat Mass Transf. **53**, 2477–2483 (2010)
23. W.A. Khan, O.D. Makinde, Z.H. Khan, MHD boundary layer flow of a nanofluid containing gyrotactic microorganisms past a vertical plate with Navier slip. Int. J. Heat Mass Transf. **74**, 285–291 (2014)
24. A.V. Kuznetsov, Bio-thermal convection induced by two different species of microorganisms. Int. Commun. Heat Mass Transf. **38**, 548–553 (2011)
25. A.V. Kuznetsov, Nanofluid bioconvection in water-based suspensions containing nanoparticles oxytactic microorganisms: oscillatory instability. Nanoscale Res. Lett. **6**, 1–13 (2011)
26. A.V. Kuznetsov, D.A. Nield, The Cheng–Minkowycz problem for natural convective boundary layer flow in a porous medium saturated by a nanofluid: a revised model. Int. J. Heat Mass Transf. **65**, 682–685 (2013)
27. A. Mahdy, Natural convection boundary layer flow due to gyrotactic microorganisms about a vertical cone in porous media saturated by a nanofluid. J. Braz. Soc. Mech. Sci. Eng. **38**, 67–76 (2016)
28. A. Malvandi, F. Hedayati, D.D. Ganji, Nanofluid flow on the stagnation point of a permeable non-linearly stretching/shrinking sheet. Alex. Eng. J. **57**, 2199–2208 (2018)
29. M.F.M. Basir, Rakesh Kumar, A.I.M. Ismail, G. Sarojamma, P.V. Satya Narayana, J. Raza, A. Mahmood, Exploration of thermal-diffusion and diffusion-thermal effects on the motion of temperature-dependent viscous fluid conveying microorganism. Arab. J. Sci. Eng. **44**, 8023–8033 (2019)
30. A.M. Megahed, MHD viscous Casson fluid flow and heat transfer with second-order slip velocity and thermal slip over a permeable stretching sheet in the presence of internal heat generation/absorption and thermal radiation. Eur. Phys. J. Plus **130**, 81 (2015)
31. S.S. Motsa, A new spectral relaxation method for similarity variable nonlinear boundary layer flow systems. Chem. Eng. Commun. **201**(2), 241–256 (2014)
32. T.J. Pedley, N.A. Hill, J.O. Kessler, The growth of bioconvection patterns in a uniform suspension of gyrotactic microorganisms. J. Fluid Mech. **195**, 223–237 (1988)
33. A. Raees, M. Raees-ul-Haq, H. Xu, Q. Sun, Three-dimensional stagnation flow of a nanofluid containing both nanoparticles and microorganisms on a moving surface with anisotropic slip. Appl. Math. Model. **40**(5-6), 4136–4150 (2016)
34. P. Rana, R. Bhargava, Numerical study of heat transfer enhancement in mixed convection flow along a vertical plate with heat source/sink utilizing nanofluids. Commun. Nonlinear Sci. Numer. Simul. **16**(11), 4318–4334 (2011)
35. S. Reddy, A.J. Chamkha, Soret and Dufour effects on MHD convective flow of Al_2O_3-water and TiO_2-water nanofluids past a stretching sheet in porous media with heat generation/absorption. Adv. Powder Technol. **27**, 1207–1218 (2016)
36. J. Reza, F. Mebarek-Oudina, O.D. Makinde, MHD slip flow of Cu-Kerosene nanofluid in a channel with stretching walls using 3-stage LobattoIiia formula. Defect Diffus. Forum **387**, 51–62 (2018)
37. A.V. Rosca, MdJ Uddin, I. Pop, Boundary layer flow over a moving vertical flat plate with convective thermal boundary condition. Bull. Malays. Math. Sci. Soc. **39**, 1287–1306 (2016)
38. H. Sardar, L. Ahmad, M. Khan, Investigation of mixed convection flow of Carreau nanofluid over a wedge in the presence of Soret and Dufour effects. Int. J. Heat Mass Transf. **137**, 809–822 (2019)

39. M. Sheikholeslami, D.D. Ganji, M.Y. Javed, R. Ellahi, Effect of thermal radiation on magnetohydrodynamics nanofluid flow and heat transfer by means of two-phase model. J. Magn. Magn. Mater. **374**, 36–43 (2015)
40. S. Siddiqa, H. Gul-E, N. Begum, S. Saleem, M.A. Hossain, R.S. Reddy Gorla, Numerical solutions of nanofluid bioconvection due to gyrotactic microorganisms along a vertical wavy cone. Int. J. Heat Mass Transf. **101**, 608–613 (2016)
41. P.R. Sobhana Babu, M. Venkata Subba Rao, K. Gangadhar, Boundary layer flow of radioactive non-Newtonian nanofluid embedded in a porous medium over a stretched sheet using the spectral relaxation method. Mater. Today: Proc. **19**(6), 2672–2680 (2019)
42. M.D. Tausif, K. Das, P.K. Kundu, Multiple slip effects on bioconvection of nanofluid flow containing gyrotactic microorganisms and nanoparticles. J. Mol. Liq. **220**, 518–526 (2016)
43. L.N. Trefethen, *Spectral Methods in MATLAB* (SIAM, Philadelphia, 2000)
44. M. Venkata Subba Rao, K. Gangadhar, P.L.N. Varma, A spectral relaxation method for three-dimensional MHD flow of nanofluid flow over an exponentially stretching sheet due to convective heating: an application to solar energy. Indian J. Phys. **92**(12), 1577–1588 (2018)
45. H. Xu, I. Pop, Mixed convection flow of a nanofluid over a stretching surface with uniform free stream in the presence of both nanoparticles and gyrotactic microorganisms. Int. J. Heat Mass Transf. **75**, 610–623 (2014)
46. H. Xu, T. Fan, I. Pop, Analysis of mixed convection flow of a nanofluid in a vertical channel with the Buongiorno mathematical model. Int. Commun. Heat Mass Transf. **44**, 15–22 (2013)